Journal of the Korean Society of Surveying, Geodesy, Photogrammetry and Cartography
Vol. 34, No. 6, 559-568, 2016
https://doi.org/10.7848/ksgpc.2016.34.6.559

ISSN 1598-4850(Print)
ISSN 2288-260X(Online)
Original article

Automatic Photovoltaic Panel Area Extraction from UAV Thermal Infrared Images

Kim, Dusik[1)] · Youn, Junhee[2)] · Kim, Changyoon[3)]

Abstract

For the economic management of photovoltaic power plants, it is necessary to regularly monitor the panels within the plants to detect malfunctions. Thermal infrared image cameras are generally used for monitoring, since malfunctioning panels emit higher temperatures compared to those that are functioning. Recently, technologies that observe photovoltaic arrays by mounting thermal infrared cameras on UAVs (Unmanned Aerial Vehicle) are being developed for the efficient monitoring of large-scale photovoltaic power plants. However, the technologies developed until now have had the shortcomings of having to analyze the images manually to detect malfunctioning panels, which is time-consuming. In this paper, we propose an automatic photovoltaic panel area extraction algorithm for thermal infrared images acquired via a UAV. In the thermal infrared images, panel boundaries are presented as obvious linear features, and the panels are regularly arranged. Therefore, we exaggerate the linear features with a vertical and horizontal filtering algorithm, and apply a modified hierarchical histogram clustering method to extract candidates of panel boundaries. Among the candidates, initial panel areas are extracted by exclusion editing with the results of the photovoltaic array area detection. In this step, thresholding and image morphological algorithms are applied. Finally, panel areas are refined with the geometry of the surrounding panels. The accuracy of the results is evaluated quantitatively by manually digitized data, and a mean completeness of 95.0%, a mean correctness of 96.9%, and mean quality of 92.1 percent are obtained with the proposed algorithm.

Keywords : Photovoltaic Panel Area Extraction, Thermal Infrared Images, Image Segmentation, UAV

1. Introduction

There are many ways of generating electricity to meet increasing energy demands. However, environmental pollution from thermal power generation and the potential risk of radiation leakages from nuclear power generation remain as risk factors for each system. Consequently, interest in eco-friendly energy has increased, and currently, related technologies are actively being developed. The photovoltaic energy generating system is a renewable energy and is of high interest. However, panels used for collecting solar energy in photovoltaic generating systems are exposed to the environment during operation. This causes short circuits due to corrosion of modules or decreases in generating efficiency due to cells being covered with dust or grime. Therefore, maintenance is required with regular inspections in order to preserve sufficient generation.

To detect photovoltaic panels with decreased generating

Received 2016. 11. 22, Revised 2016. 12. 14, Accepted 2016. 12. 28
1) Member, Korea Institute of Civil Engineering and Building Technology, ICT Convergence and Integration Research Institute (E-mail: dusikkim@kict.re.kr).
2) Corresponding Author, Member, Korea Institute of Civil Engineering and Building Technology, ICT Convergence and Integration Research Institute (E-mail: younj@kict.re.kr).
3) Korea Institute of Civil Engineering and Building Technology, ICT Convergence and Integration Research Institute (E-mail: ckim@kict.re.kr).

efficiency, manual analysis methods and performance measurement methods based on I-V curve analysis can be implemented. However, for the maintenance of large-scale photovoltaic power plants, manual analysis methods are expensive and time-consuming in detecting malfunctioning panels. The performance measurement method is difficult for monitoring the generated quantity of each panel. Hence, developing technology that can overcome the limits of existing maintenance methods is required.

Photovoltaic panels with decreased generating efficiency show higher temperatures in thermal infrared images compared to normal panels. Therefore, using thermal infrared images allows non-destructive testing for malfunctioning panels while the photovoltaic power plant is under operation. Furthermore, fast and accurate detection of malfunctioning panels is possible since it can also detect micro cracks that cause reduced generating efficiency, which are difficult to detect with the existing manual analysis method. These technological advantages are used to design the handheld thermal infrared cameras applied to test malfunctioning panels and for maintenance (Bazilian *et al*., 2002).

Recently, as UAVs have become popular, technologies for monitoring photovoltaic power plants by mounting thermal infrared cameras on UAVs have been developed (Buerhop and Scheuerpflug, 2014; Grimaccia *et al*., 2015; Quarter *et al*., 2014). Technologies developed until now were limited to detecting malfunctioning panels by manually analyzing the aerial thermal infrared images. The drawback of this technique is that it is time consuming, since analysis had to be done for every single image. Therefore, using computer vision algorithms to automatically detect malfunctioning panels is necessary. If an automatic detection technology is developed, malfunctioning panels can be selected quickly, without any manual decision-making.

In order to detect malfunctioning panels from aerial thermal infrared images, selecting the region of interest (i.e. the photovoltaic panel areas) from the images, is required. Here, extracted images must be able to form polygons for each panel, in order to extract the malfunctioning panels using profile analyses. The analyzed results of the edge extraction method, previously developed by Canny (Canny, 1986), Sobel etc., proved difficult for the single polygon formation around a panel area due to noise within and around the panel. Furthermore, applying the Hough operator line transform method resulted in excessive extraction of straight lines. This required applying manually simulated conditions, inappropriate for an automatic panel area extraction algorithm. Therefore, as a primary technique required to automatically extract malfunction panels from the thermal infrared images, we developed an algorithm for the automatic extraction of panel areas, expressed in a polygon format.

2. Panel Area Extraction Algorithm

In this study, thermal infrared images obtained previously

Table 1. The specification of the FLIR T620

Subsection	Specification
Frame Rate	30Hz
Field of View	25° × 19°
Minimum Focus Distance	0.25 m
Spectral Range	7.5 to 14μm

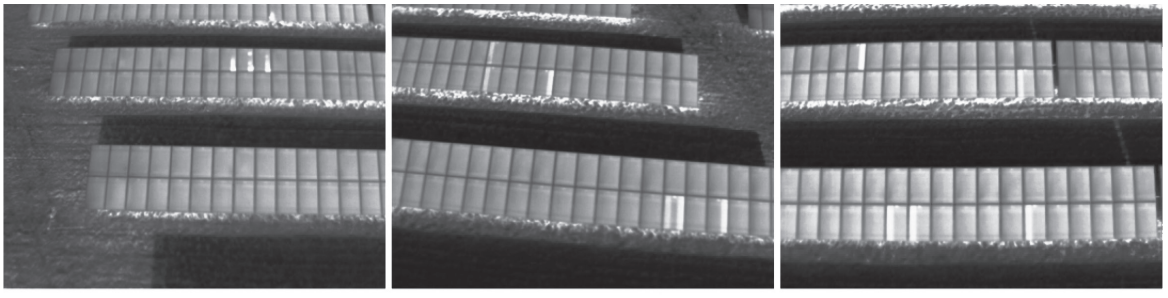

(A) **(B)** **(C)**

Fig. 1. Sample of thermal infrared images (source: www.kitawa.de)

from a relevant manufacturer are used. Company Paul Kitawa from Germany developed a drone loaded with the FLIR T620 thermal infrared camera, for photovoltaic power plant monitoring. Samples of thermal infrared images of the photovoltaic power plant taken using the drone are provided on Paul Kitawa's website (www.kitawa.de). The specifications of the FLIR T620 are presented in Table 1. From these samples, three images (Fig. 1) with dimensions of 640×480 pixels are selected as sample data. The specifications of the UAV are not provided on the website.

As shown in Fig. 1, photovoltaic panels can be identified with their higher temperatures compared to their surroundings. Most of the panel areas present roughly a steady temperature and the panel edges show lower temperatures compared to the panel area. Among all sample images, more than one hotspot panel is presented, and every panel array shows sections of high temperature in the lower part. However, turning the image to gray scale and eliminating blank spaces based on certain thresholds of intensity could not eliminate the noise in the lower part of the array. Therefore, an image segmentation technique was applied to extract individual polygons for each enclosed panel area.

The panel area extraction algorithm developed in this paper has a process of four stages, as described in Fig. 2. Firstly, candidates of the photovoltaic panel boundaries are extracted. To determine the edges of the photovoltaic panels, we use horizontal and vertical filters to emphasize the linear features. After that, we applied a modified hierarchical histogram clustering method, proposed in Youn *et al*. (2008), to select the maximum probability candidates. Secondly, photovoltaic array areas are detected with thresholding and morphological filtering. Thirdly, initial panel areas are extracted using exclusion editing. Among the candidates of panel boundaries, the candidates, which are located in the photovoltaic arrays, are excluded in this step. After this process, we can determine each panel's initial polygon. However, these polygons still have an over-extracted area in the lower part of the photovoltaic arrays. Therefore, as a last step we refine the panel areas with the geometry of the surrounding panels. The case of (B) in Fig. 1 is used as an example to show the process of extracting the panel areas.

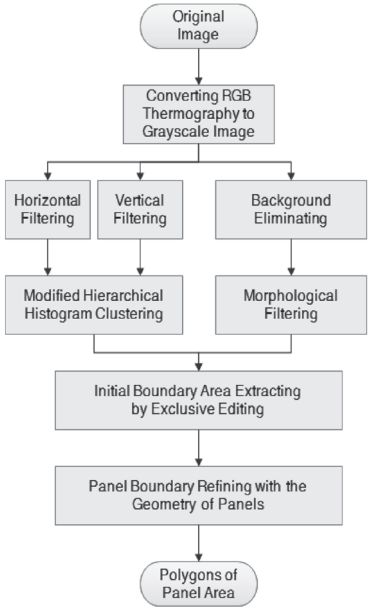

Fig. 2. Flow chart of panel area extraction algorithm

2.1 Extracting candidates for panel boundaries

The purpose of this step is producing candidates for panel

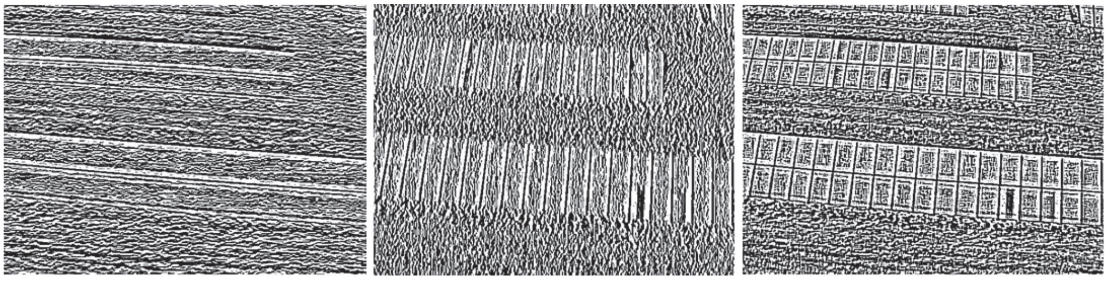

(A) **(B)** **(C)**

Fig. 3. Results of applying horizontal and vertical filtering on a sample image. (A) Horizontal filtering result, (B) Vertical filtering result, and (C) Result of combining horizontal and vertical filtering

boundaries which express the boundaries between panels. As seen in Fig. 1, the boundaries of the panels show obvious linear features. Therefore, we can select the pixels with maximum differences in intensities as candidates of panel boundary points. The original image is converted into grayscale, and filtering masks are applied. A 5×5 pixel window was applied as the space filter mask to apply horizontal and vertical filtering. Horizontal and vertical masks are expressed as hw and vw, as shown in eq. (1). The results obtained using the masks are shown in Fig. 3 (A) and (B), and the two results are combined in Fig. 3(c). In Fig. 3, bright pixels represent the higher correlation values.

$$\mathrm{hw}=\begin{bmatrix}-1&-1&-1&-1&-1\\-1&-1&-1&-1&-1\\4&4&4&4&4\\-1&-1&-1&-1&-1\\-1&-1&-1&-1&-1\end{bmatrix},\quad \mathrm{vw}=\begin{bmatrix}-1&-1&4&-1&-1\\-1&-1&4&-1&-1\\-1&-1&4&-1&-1\\-1&-1&4&-1&-1\\-1&-1&4&-1&-1\end{bmatrix} \quad (1)$$

As shown in Fig. 3, applying the vertical and horizontal filters emphasized the linear features in each direction. Combining the filters resulted in a precise outline of the panels. Therefore, by detecting the pixels that show strong linear features as in Fig. 3 (A) and (B), we can clearly extract the candidates for panel boundaries.

In Fig. 4, the intensity profile at the location of the straight line in the gray scale image on the left is shown in graph (A) on the right. In graph (A), periodic signals that have a low intensity indicate the panel boundaries. Graph (B) shows the correlation (Vertical Filter Correlation, VFC) profile for the vertical filter result (Fig. 3 (B)) at the same location of the straight line in the gray scale image. Fig. 4 (C) presents the absolute value of VFC. Comparing Fig. 4 (A) with Fig. 4 (C), we know that the location of peak points in the profile graphs indicate the boundaries of the panels. To find the peak points, we apply the modified hierarchical histogram-clustering method, proposed in Youn *et al.* (2008), at the absolute value of VFC. Firstly, the highest peak in the profile graph is determined. Pixel discrepancies less than the threshold (±30 pixels for the horizontal filter and ±20 pixels for the vertical filter) from the peak are checked as one set. The threshold value is determined considering the size of the panels, since the peaks correspond to the edges of the panels. The next highest peak is then determined, ignoring the previously checked sets. This process continues until all pixels are checked. The established peaks, in absolute value of VFC, are presented in Fig. 4 (C) as circles. Comparing Fig. 4 (A) with (C), the peaks points agree with the panel boundaries. To obtain more accurate results, profiling directions should be parallel with panel array edges.

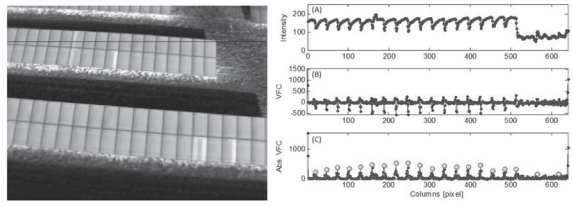

Fig. 4. Left : Gray scale image and profile location (straight line), Right : (A) intensity values profile, (B) VFC, and (C) peak results using absolute values of VFC

We apply the modified hierarchical histogram-clustering method to the results of the vertical and horizontal filtering. The peak points are then detected for every row and column, and the position of the peak points is stored in a void image. Fig. 5 (A) presents the detected peak points. In Fig. 5 (A), some pixels are connected, and others are not. Panel boundaries have connected pixel form. Therefore, pixels are required to enclose the outcome as much as possible by connecting the adjacent pixels. We apply a circular filter with the size of 3 pixels using an algorithm proposed by Corke (2011) to make the connections in the initial frame image. 3 pixels are minimum size of the circular filtering. Fig. 5 (B) shows the results after applying the circular filter.

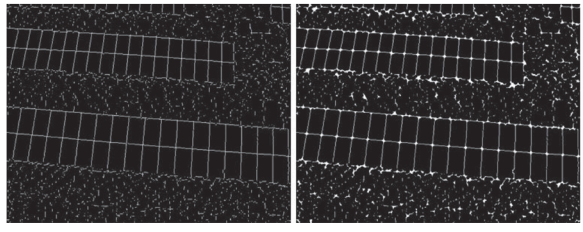

(A) **(B)**

Fig. 5. Extracted candidates of the panel boundaries; (A) detected peak points and (B) closed geometry of the detected peak points

2.2 Extracting photovoltaic arrays

The prior candidates from the panel boundaries extraction

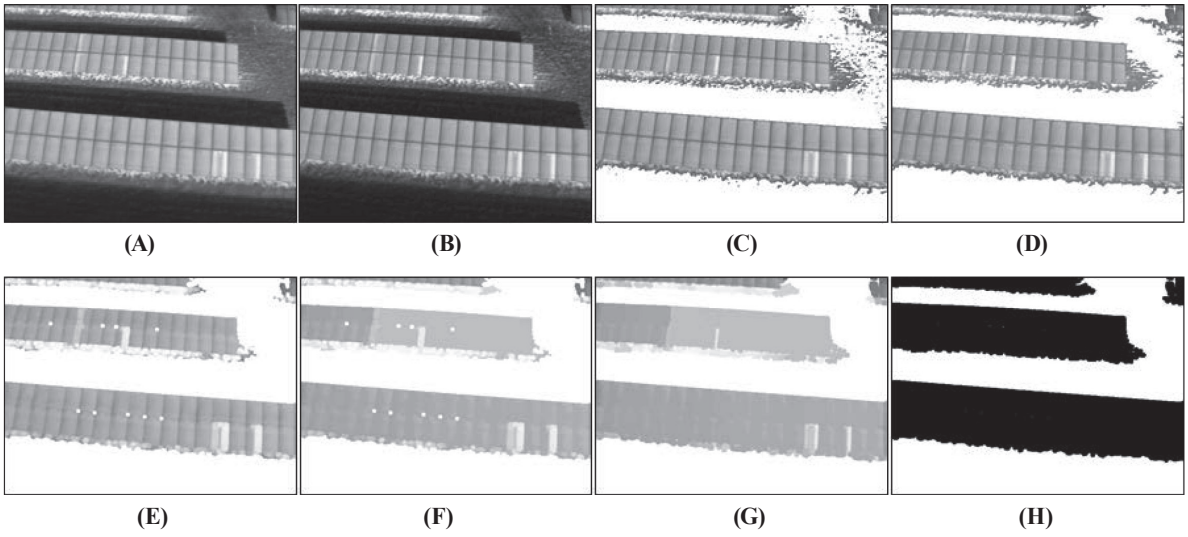

Fig. 6. Photovoltaic arrays extraction process; (A) original image, (B) converted gray scale image, (C) background elimination by thresholding, (D) fill holes, (E) background pixel dilatation, (F) fill holes, (G) background pixel erosion and (H) the final image of the photovoltaic arrays areas

results still need to be refined by exclusion editing with some obvious non-panel boundaries. In the scene under study, readily detectable non-panel boundaries are located in the background of the photovoltaic arrays. In this section, we describe the process of extracting photovoltaic array areas. Fig. 6 shows the results of the process.

The first step for extracting the photovoltaic area is eliminating approximate background areas by thresholding. The original image is converted into grayscale (Fig. 6 (A) and Fig. 6 (B)). Generally, when a thermal infrared camera captures a photovoltaic power plant while under operation, the panel temperature shows up higher than the background. Therefore, since the intensity of the panel area is higher than the background in the thermal infrared images, a certain threshold value is assigned to determine the background area. Here, the threshold value is set to 100, and as a result, it is possible to roughly eliminate the background area, as shown in Fig. 6 (C). The selected threshold value is determined by a heuristic approach. The threshold value selection for generating a binarized image is complex and should be improved.

However, in Fig. 6 (C), an area with geothermal heat in the background creates noise, and hence a certain area is not removed with the selected threshold value. Since the purpose of extracting a photovoltaic array area is to exclude candidates of panel boundaries which are located in the background, noise within the photovoltaic array area or blank spaces in the background due to noise should be excluded. Consequently, an additional noise filtering is necessary to remove this area, and a morphological image processing technique, introduced by Gonzalez *et al*. (2004), is used to remove the noise.

Firstly, the hole in Fig. 6 (C) in the background area is filled in and the dilatation of the background area allows for the removal of the remaining noise (D and E in Fig. 6). Holes remaining after the dilatation of the background are filled up and background pixel erosion is applied (F and G in Fig. 6) again. Lastly, only areas with intensity value of 0 are selected to extract the background area, as shown in Fig. 6 (H). The approximate areas of the photovoltaic array are obtained using this algorithm. However, noise around the photovoltaic arrays is still present.

2.3 Extracting initial panel area

In Section 2.1, the candidates for panel boundaries were extracted. However, many candidates were located in the background of the photovoltaic array areas. Photovoltaic array areas were detected in Section 2.2. Therefore, we can

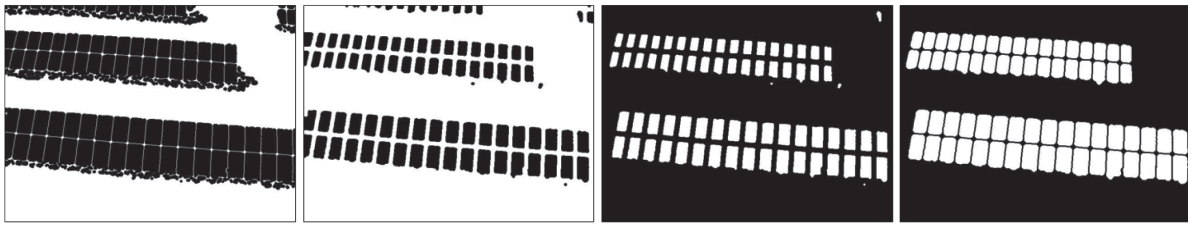

(A) (B) (C) (D)

Fig. 7. (A) Initial panel area extraction process; exclusion editing, (B) pixel dilatation to get closed geometry, (C) inverse transformation of image and (D) image of initial panel areas

apply the exclusion editing of the provisional candidates of panel boundaries using the photovoltaic areas as a blocking mask. For each candidate pixel, we make a pixel set of the corresponding line and sample coordinates. Comparing this set with the raster exclusion mask, if a candidate pixel coincides with the mask, then such pixels are eliminated.

Fig. 7 (A) shows the results of the exclusion editing. This image still contains noise in the lower region of the panel arrays. Therefore, connecting adjacent pixels to form a closed geometric shape is necessary, as with the last stage of extracting candidates for panel boundaries. Since the overall outline is complete, dilatation of white areas effectively produces an enclosed object, as shown in Fig. 7 (B). Since morphological image processing recognizes white areas as a region of interest, inversing produces images such as in Fig. 7 (C). Objects not expressing an entire panel are eliminated from the region of interest and only parts that show an entire panel in the image are used for analysis. Fig. 7 (C) shows the image still containing noise, and by using the number of pixels that make up each object, objects consisting of less than 750 pixels are eliminated from the region of interest. In the images, the number of pixels that make up one panel is approximately between 800 and 2000. The threshold value of 750 pixels is determined considering the minimum size of the panel size. Lastly, dilatation of objects gives the initial panel image, as shown in Fig. 7 (D).

2.4 Refining panel area

Examining the extracted initial panel areas in Fig. 7 (D), some panels contain noise, particularly in the lower part of the photovoltaic arrays, due to the radiation heat from the ground. Those above the extracted section can be refined using the geometric differences between the surrounding panels. Fig. 8 (A) presents the results of the overlapping extracted initial panel areas with the original image. In the box area of Fig. 8 (A), the over extraction of certain panels is shown in the lower part of the panel array. This phenomenon is thought to be from the noise in the lower regions of the panel arrays, where the boundaries between the panel and the ground are uncertain. Performing profile analysis on the panel polygons extracted in this condition may have resulted in error, whereby functioning panels are selected as malfunction panels due to the noise in the lower regions of the panel arrays.

In order to avoid this error, refining the extracted panel boundaries is necessary. Real panel and photovoltaic arrays are rectangular types; however, panel arrays are not expressed with a straight line in the images acquired by UAV due to lens distortion. Since it is impossible to refine all panel arrays with a single straight line, the lowest points on each side of the concerned panel boundary are connected to eliminate the over extracted area. Fig. 8 (B) presents the initial panel areas for the box area in Fig. 8 (A) and the concept of the refining algorithm. For example, to eliminate the over extracted area of panel 32 in Fig. 8 (B), a straight line is connected between the bottoms parts of the rectangular areas of panels 31 and 33. Next, the areas of panel 32 below the line are eliminated. The rectangular area is formed based on the maximum and minimum pixel coordinates that lie within the panel polygon. Since the over extraction of area only happens at the lower region of the panel arrays, the algorithm is only applied to this region. This technique can only be applied to photovoltaic power plants that use the same sized panels, as the boundaries of

the panels on each side of the concerned panel are used as a reference for the panel area. If the exterior orientation parameters of the sensor are known, then a refining process may be applied to the lower part (south side of the panel array), since such radiation effects would not occur in the north side of the panel array due to shadows. However, the refining process is applied to the upper and lower part of the panel arrays, since the exterior orientation parameters are not known in this experiment.

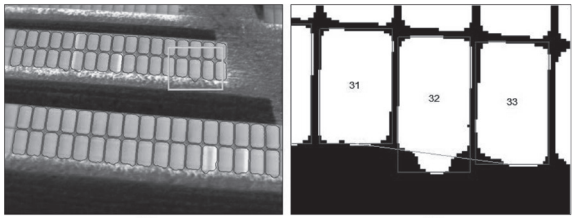

(A) **(B)**

Fig. 8. (A) Overlapping extracted initial panel areas with original image and (B) concept of refining algorithm

Fig. 9 shows the results of applying the panel area extraction algorithm developed in this study, to the sample images in Fig. 1. The panel area extraction algorithm recognized individual panels within the image, as long as the entire panel was captured and produced ROI polygons for each panel area, as shown in Fig. 9.

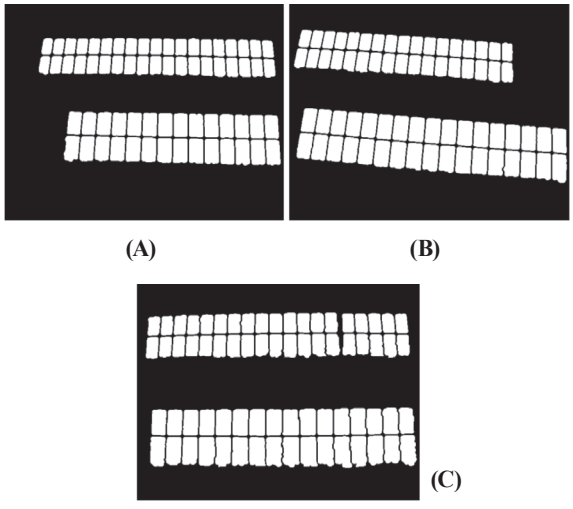

(A) **(B)**

(C)

Fig. 9. Panel area extraction results of sample images

3. Panel Area Extraction Algorithm Performance Evaluation

For performance evaluation of the algorithm, the derived model extracted from the algorithm developed in this study, and the manually digitized panel boundary (reference model) are compared. The performance evaluation technique introduced by McGlone *et al*. (2004) and Youn *et al*. (2008) is used for a quantitative evaluation. The evaluation method assesses factors such as completeness, correctness, and quality, to evaluate the accuracy of the area extraction. Each factor is calculated with the equations below.

$$\text{Completeness} = \frac{TP}{TP+FN} \tag{2}$$

$$\text{Correctness} = \frac{TP}{TP+FP} \tag{3}$$

$$\text{Quality} = \frac{TP}{TP+FP+FN} \tag{4}$$

Here, TP (True Positive), FP (False Positive), and FN (False Negative) each indicate the number of pixels for each case, when the extracted panel area results are compared with the reference model.

Fig. 10 shows an example to explain the performance evaluation algorithm for panel extraction in detail. In each figure, the solid squares represent the area of the reference model, and the boundaries drawn with thick lines represent the area of the derived model. As shown in Fig. 10, TP shows an area in agreement between the derived model and reference model, FP indicates extracted areas that were not included in the reference model, and FN indicates areas not extracted despite being part of the reference model area. Completeness indicates the number of pixels that were selected among the pixels that were supposed to be selected as the panel area, using the reference model as a reference. Correctness indicates the ratio of correctly extracted pixels in the derived model. An indicator that represents these two factors together is quality, denoting the ratio of correctly extracted pixels out of the combined pixels from the derived and reference models. The assessment of this factor can quantitatively represent completeness and correctness of the algorithm for panel area extraction.

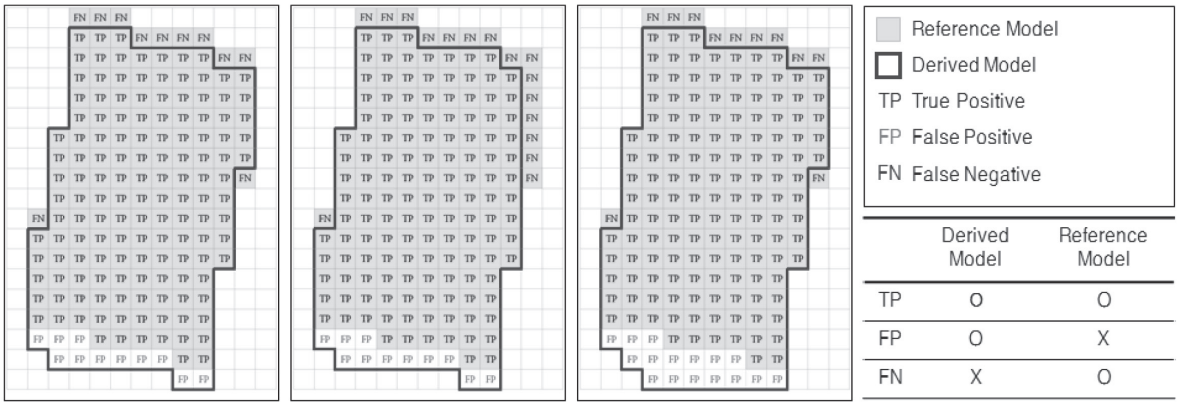

(A)TP: 139, FN: 11, FP: 11 (B)TP: 135, FN: 16, FP: 11 (C)TP: 139, FN: 11, FP: 16

Fig. 10. Example of performance evaluation of the panel area extraction algorithm

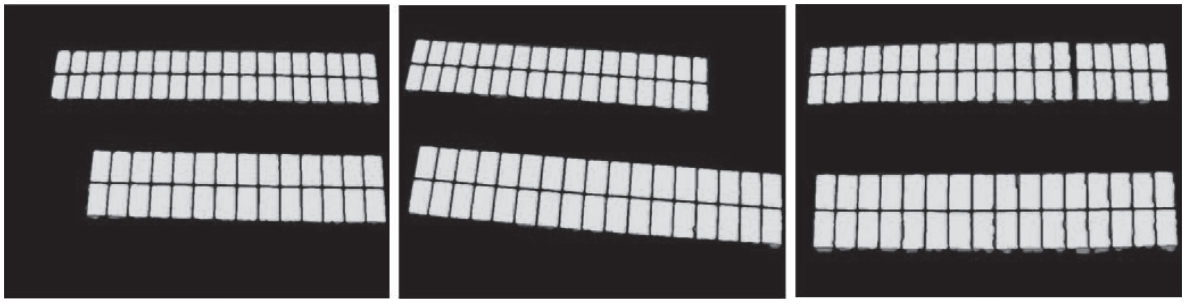

(A) **(B)** **(C)**

Fig. 11. Results of the performance evaluation on the panel area extraction algorithm (green: TP, blue: FN, red: FP)

Table 2. Panel area extraction algorithm performance evaluation results

Case	TP	FN	FP	Completeness	Correctness	Quality
	[pixels]			[%]		
A	81,655	4,714	1,881	94.5	97.8	92.5
B	95,995	4,074	2,538	95.9	97.4	93.6
C	108,258	6,317	5,278	94.5	95.4	90.3
Mean				95.0	96.9	92.1

Fig. 11 shows the results of the evaluation of panel area extraction on three sample images using this method. The green represents TP, blue represents FN, and red denotes FP. The performance evaluation results of three images show that FN frequently occurred in the upper region of the photovoltaic arrays, whereas FP frequently occurred in the lower region of the photovoltaic arrays. This means that the algorithm could not describe the panel boundary as precisely as the manually digitized boundary. Furthermore, it means that uncertainty prevailed in determining the lower boundary of photovoltaic arrays due to noise. Particularly in Fig. 11 (C), FP pixels are more common compared to the other two images. This is thought to be a result of noise in the lower region of the photovoltaic arrays.

Results in Fig. 11 are quantitatively analyzed in Table 2. When the number of pixels used to extract panel areas is counted using TP, FN, and FP, areas occupied by the panels are different, in the order of C, B, and A. Results of A and

B show over 94% of completeness, over 97% of correctness and over 92% of quality. However, results of C show lower values compared to A and B, with completeness of 94.5% and correctness of 95.4%. Additionally, quality is low at 90.3%, confirming that the increase in uncertainty in extracting panel areas is due to noise effects in the lower region of the photovoltaic arrays in image C.

4. Conclusions

In this paper, we proposed a photovoltaic panel area extraction algorithm from thermal infrared images acquired using a UAV. Candidates for panel boundaries were extracted with vertical filtering, horizontal filtering, and a modified hierarchical histogram clustering method. Non-panel candidates were excluded with the results of the photovoltaic array detection. Initial panel boundaries were obtained via the application of an additional morphological algorithm. Finally, panel boundaries were refined with the geometry of surrounding panels. The algorithm developed in this study to extract panel areas from aerial thermal infrared images of photovoltaic power plants was applied to three samples images. As a result, the algorithm was able to produce panel areas at an average quality of 92.1 %. Although the panel boundaries were not perfectly extracted in a linear format, noise surrounding and within the panels were effectively removed, allowing individual panel recognition, which was required for analyzing malfunctioning panels. In order to apply the developed panel extraction algorithm to automated monitoring systems for photovoltaic power plants, functions that allow automatic extraction from images with varying resolutions and measuring heights must be added. The three sample images selected in this study had similar intensity characteristics and panel sizes. However, if image scale or intensity span is changed, it should still be possible to change the fixed variables in this algorithm (pixel discrepancies for the modified hierarchical histogram clustering method, thresholding value for extracting photovoltaic array areas etc.). Thus, the algorithm should be revised using images obtained through actual experiments. Performing image labeling on ROI polygon images obtained from this algorithm allowed the recognition of individual panels. This meant that based on information of each panel area, profile analysis on the intensities for each panel was possible. Here, it was anticipated that panels with hotspots would have relatively larger fluctuations in the profile compared to regular panels. Therefore, for the advancement of the automated monitoring system of photovoltaic power plants, an algorithm that detects malfunctioning panels based on the intensity or temperature profiles should be developed through continuous research. The proposed algorithm is applied to the thermal infrared images acquired by a UAV on the assumption that the exterior orientation parameters of the sensors are not known. Without the exterior orientation parameters, the threshold values for the hierarchical histogram clustering method and the elimination of non-panel areas are not automatically determined. If the parameters are determined, then the threshold values may be automatically determined, considering the size of the panels.

Acknowledgments

This study was conducted under the support by the project of “Development of high Efficiency Solar Road Power Generation Technology” funded by the Korea Institute of Civil Engineering and Building Technology.

References

Bazilian, M.D., Kamalanathan, H., and Prasad, D.K. (2002), Thermographic analysis of a building integrated photovoltaic system, *Renewable Energy*. Vol. 26, No. 3, pp. 449-461.

Buerhop, C. and Scheuerpflug, H. (2014), Field inspection of PV-modules using aerial, drone-mounted thermography, *Proceedings of the 29th European Photovoltaic Solar Energy Conference and Exhibition*, EUPVSEC 2014, 23-25 September, Amsterdam, Netherlands, pp. 2975-2979.

Canny, J. (1986), A computational approach to edge detection, *IEEE Transactions on Pattern Analysis and Machine Intelligence*, Vol. 8, No. 6, pp. 679–698.

Corke, P. (2011), *Robotics, Vision and Control: Fundamental algorithms in MATLAB Vol. 73*, Springer: Heidelberg,

Berlin, pp. 344-346.

Gonzalez, R.C., Woods, R.E., and Eddins, S.L. (2004), *Digital Image Processing using Matlab*, Pearson Prentice Hall, Upper Saddle River, NJ, pp. 334-425.

Grimaccia, F., Aghaei, M., Mussetta, M., Leva, S., and Quater, P.B. (2015), Planning for PV plant performance monitoring by means of unmanned aerial systems (UAS), *International Journal of Energy and Environmental Engineering*, Vol. 6, No. 1, pp. 47-54.

McGlone, J.C., Mikhail, E.M., and Bethel, J.S. (2004), *Manual of Photogrammetry 5th Edition*, ASPRS, Bethesda, MD, pp. 969-970.

Quater, P.B., Grimaccia, F., Leva, S., Mussetta, M., and Aghaei, M. (2014), Light Unmanned Aerial Vehicles (UAVs) for Cooperative Inspection of PV Plants, *IEEE Journal of Photovoltaics*, Vol. 4, No. 4, pp. 1107-1113.

Youn, J., Bethel, J.S., Mikhail, E.M., and Lee, C. (2008), Extracting Urban Road Networks from High-resolution True Orthoimage and Lidar, *Photogrammetric Engineering and Remote Sensing*, Vol. 74, No. 2, pp. 227-237.